The absence of correlations between a clinical classification and ultrastructural findings in amelogenesis imperfecta

Birgitta Bäckman, Ted Lundgren, E. Urban Engström, Lena K. L. Falk, Jan M. Chabala, Riccardo Levi-Setti and Jörgen G. Norén

Department of Pedodontics, Faculty of Odontology, University of Umeå, Umeå, and Department of Pedodontics, Faculty of Odontology, University of Göteborg, and Department of Physics, Chalmers University of Technology, Göteborg, Sweden, and Enrico Fermi Institute, University of Chicago, Chicago, Illinois, USA

Bäckman B, Lundgren T, Engström EU, Falk LKL, Chabala JM, Levi-Setti R, Norén JG. The absence of correlations between a clinical classification and ultrastructural findings in amelogenesis imperfecta. Acta Odontol Scand 1993;51:79–89. Oslo. ISSN 0001–6357.

This study was performed to examine whether a clinical classification of different phenotypes of amelogenesis imperfecta could be discernible at the ultrastructural level. Seventeen primary teeth from 16 children with hypomineralization, hypomaturation, or hypoplastic variants of the disease were collected for histologic studies of the enamel by means of polarized light microscopy, scanning electron microscopy (SEM), and secondary ion mass spectrometry (SIMS). Polarization microscopy showed that the enamel was hypomineralized; in six teeth a wavy configuration of the enamel prisms also appeared. Three histomorphologic main types could be discerned. In 10 of the teeth extensive hypomineralization of the bulk of the enamel was found. One tooth had an unusually thick enamel with only a thin normally mineralized surface layer. SIMS images showed less pronounced signals from Ca^{2+} and Na^{+} but with stronger signals from Cl^{-} and CN^{-}, representing the organic component of enamel. The SEM images showed an irregular prism pattern with marked interprismatic areas. Irrespective of the clinical appearance or the hereditary pattern the main findings were hypomineralized enamel with or without wavy bands. Neither of the analytical methods used in this paper distinguishes between the clinical phenotypes of amelogenesis imperfecta. □ *Amelogenesis imperfecta; dental enamel; genetics; microscopy, electron, scanning; secondary ion mass spectrometry, spectrum analysis, mass*

Jörgen G. Norén, Department of Pedodontics, Faculty of Odontology, Medicinaregatan 12, S-413 90 Göteborg, Sweden

Amelogenesis imperfecta (AI) is defined as a genetically determined defect affecting enamel formation and may be associated with other ectodermal or systemic disorders (1, 2). AI is characterized by a variability of clinical expression and by genetic heterogeneity (3–6). The amelogenin gene has been localized to the X chromosome (7), and X-linked amelogenesis imperfecta has been mapped to the same region (8) with a deletion in the gene in one family (9). The prevalence stated for AI varies from 1:8000–14,000 (4, 10, 11) to 1.4:1000 (12) depending on the diagnostic criteria and the demographic character of the investigated population.

Different histologic techniques have been applied in the examination of teeth with AI. By microradiography, a generalized disturbance of the amelogenesis has been established, manifested by the simultaneous occurrence of both hypoplasias and areas of hypomineralization in the enamel independent of the predominant clinical manifestation (13–15). By light and polarization microscopy and by transmission electron microscopy and scanning electron microscopy (SEM) various findings have been described in enamel from AI patients (16–28). Secondary ion mass spectrometry (SIMS) is an established technique for measuring surface and in-depth elemental distributions in dental hard tissues (29–31). Two basic types of instruments are capable of generating mass-resolved secondary ion images: scanning ion microprobes (SIM) and direct-imaging ion probes.

With developments in SIM, secondary ion

(ISI) and secondary electron (ISE) imaging can be obtained which is comparable, in detail and resolution, with those obtained by SEM.

The aim of this investigation was to examine whether a clinical classification of AI also could be detected at the histologic and chemotopographic level by means of polarized light microscopy and imaging SEM and SIMS.

Materials and methods

The material comprised 17 exfoliated primary teeth from 16 children with AI documented in earlier studies (5, 12, 15). The children belonged to either of 14 families with a known inheritance pattern of AI (5, 6). On the basis of the clinical manifestation of AI, the teeth were classified in accordance with the morphologic criteria stated by Witkop & Sauk (3). The distribution of families, patients, teeth, and inheritance pattern is presented in Table 1.

Table 1. Distribution of examined teeth in accordance with Bäckman & Holmgren (5), including tooth number, clinical classification, family number, and inheritance pattern

Tooth no.	Clinical variant of AI*	Family no.	Inheritance pattern†
51	Local hypoplastic	7	AD
51	Local hypoplastic	9	AD
51	Local hypoplastic	9	AD
53	Pitted hypoplastic	17	AD
63	Rough hypoplastic	46	S
83	Rough hypoplastic	48	S
63	Hypomaturation	34	AR
62	Hypomaturation	42	S
61	Hypomaturation	28	AD
51	Hypomaturation	31	AD
83	Hypomaturation	31	AD
65	Hypomineralization	29	AD
53	Hypomineralization	2	AD
54	Hypomineralization	2	AD
81	Hypomineralization	30	AD
61	Hypomineralization	43	S
64	Hypomineralization	44	S

* AI = amelogenesis imperfecta.

† AD = autosomal dominant inheritance pattern; AR = autosomal recessive inheritance pattern; S = spontaneous case, no AD and no AR.

Preparation of teeth and polarized light microscopy

All teeth, representing all clinical variants (Table 1), were embedded in methylmethacrylate, and sagittal bucco-lingual sections 80–100 μm thick were prepared with a Leitz low-speed saw microtome (32). The sections were polished with diamond paste and examined dry in air and after water imbibition in polarized light using an Olympus BH polarizing microscope with strain-free objectives.

SIMS analysis

The high-resolution SIM used in this study (UC-HRL SIM) has been described in detail elsewhere (29-31), and only a short description will be given here. The instrument uses a liquid gallium ion source to produce a 40-keV, 30-pA primary ion probe, focused to a spot approximately 50 nm in diameter. The images presented in this article were derived from scans containing 1024 × 1024 probe settings, and the detected signal was displayed as individual counts on a cathode ray tube.

Sections from four teeth were imaged by SIMS from families 29, 31, 48 and 44, representing four clinical variants of AI (Table 1). After being re-embedded in methylmethacrylate the free surface of the specimen was polished with diamond paste. The samples were coated with a gold layer by means of vacuum deposition, to prevent electric charging artefacts. Imaging of tooth enamel, which is highly insulating, requires an unusually thick Au coating (approximately 20 nm). Even with this precaution, repeated high-magnification imaging (20 × 20 μm^2 field of view) was prevented because of rapid charge accumulation.

The images were obtained from an area of 80 × 80 μm from the section with thin enamel and from an area of 160 × 160 μm from the other tooth analyzed by SIMS.

SEM

Sections from two teeth were examined by SEM: one specimen from family 44 (also examined by SIMS) and one specimen from

family 29 (Table 1). After evaporation of a thin carbon layer onto the specimen surfaces, to avoid charging under the electron beam, the specimens were characterized by means of CamScan 4S-80DV scanning electron microscope. The SEM images presented in this paper were obtained from backscattered electrons. Images were obtained in 400× and 1000× magnification.

Results

Polarized light microscopy

The neonatal line was seen in 12 of the ground sections from the 17 teeth, thus enabling us to distinguish the prenatal enamel from the postnatal. The neonatal line appeared positively birefringent as seen dry in air and remained positively birefringent after water imbibition.

Areas of hypomineralization of various extents were found in all examined teeth, being independent of the clinical classification. On the basis of the morphologic appearance in the polarizing microscope the teeth could be divided into three groups:

Teeth (10 of 17) showing only hypomineralized areas in the bulk of the enamel. In all specimens a negatively birefringent surface zone reflecting a normal surface mineralization could be observed (Fig. 1). This surface zone varied in thickness. Deep to the surface zone a positively birefringent area was seen, varying in its extension within the tissue. This hypomineralized zone remained positively birefringent after water imbibition, indicating a degree of porosity between 1% and 5%. In all specimens a thin negatively birefringent zone was seen adjacent to the dentinoenamel border. Defects with rough borders in the incisal part were seen in three of the specimens, reflecting chipping of the enamel. Deep to the defects the enamel had a high degree of pore volume distribution. One sample had an enamel defect in the form of a reduced thickness of the enamel, with rounded borders, representing an enamel hypoplasia. The bottom of the defect corresponded to the neonatal line in the cervical part of the tooth, indicating that the disturbance occurred at the time of birth.

In six teeth from five patients the bulk of the enamel appeared positively birefringent, as examined dry in air, with bands of 'wavy' appearance, whereas the surface zone appeared negatively birefringent. The positive birefringence remained after water imbi-

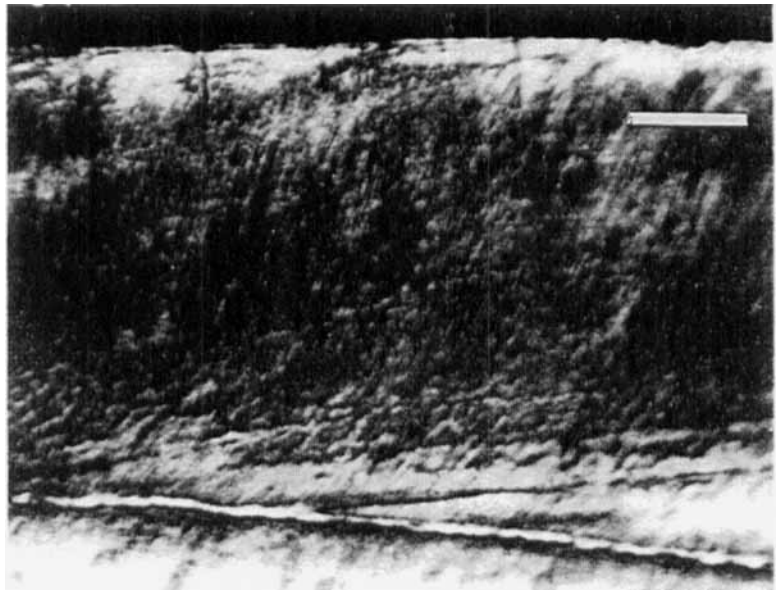

Fig. 1. Ground section of a primary tooth as seen dry in air in polarized light. Beneath a normally mineralized surface, the bulk of the enamel is hypomineralized. The bar corresponds to 1 mm.

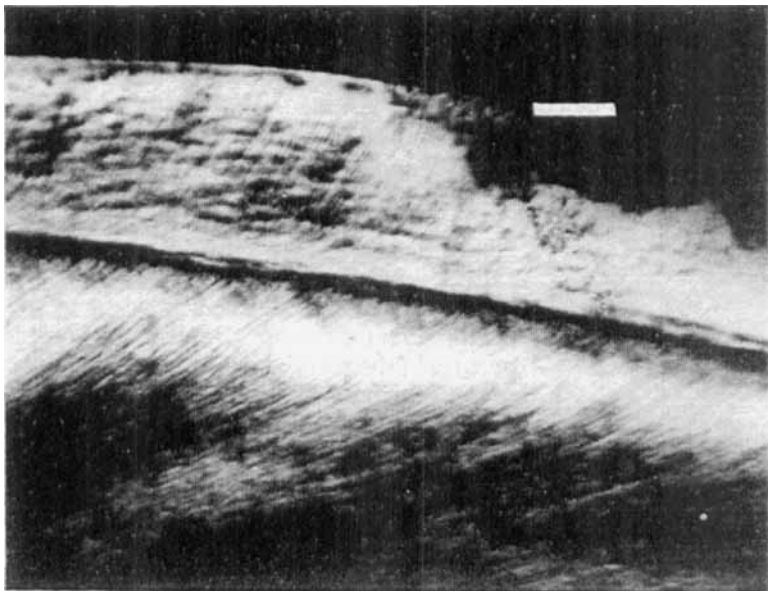

Fig. 2. Ground section of a primary tooth as seen dry in air in polarized light, showing enamel with an irregular appearance. Chipping of the enamel is seen at the incisal part of the tooth. The bar corresponds to 500 μm.

bition. Chipping of the enamel along the 'wavy bands' was noted in the incisal parts of four of the six teeth (Fig. 2).

One tooth had enamel that was thicker than normal and with a pronounced cervical prominence (Fig. 3). The enamel appeared positively birefringent with a thin negatively birefringent surface zone. The positive birefringence of the enamel remained in its major part after water imbibition. Bands resembling the Hunter–Schreger bands found in permanent enamel were also observed. These bands remained positively birefringent after water imbibition.

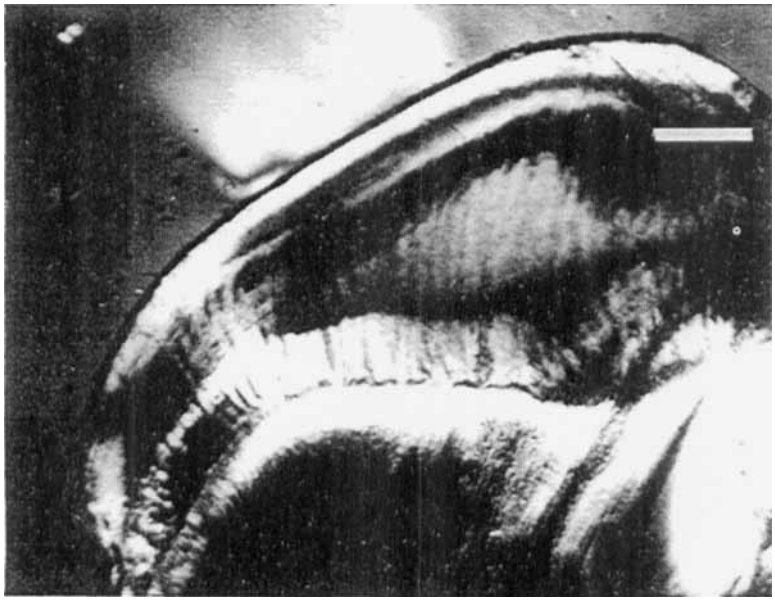

Fig. 3. Ground section of a primary tooth with an unusually thick enamel. The thin surface zone has a normal mineralization, whereas the bulk of the enamel is hypomineralized. The bar corresponds to 250 μm.

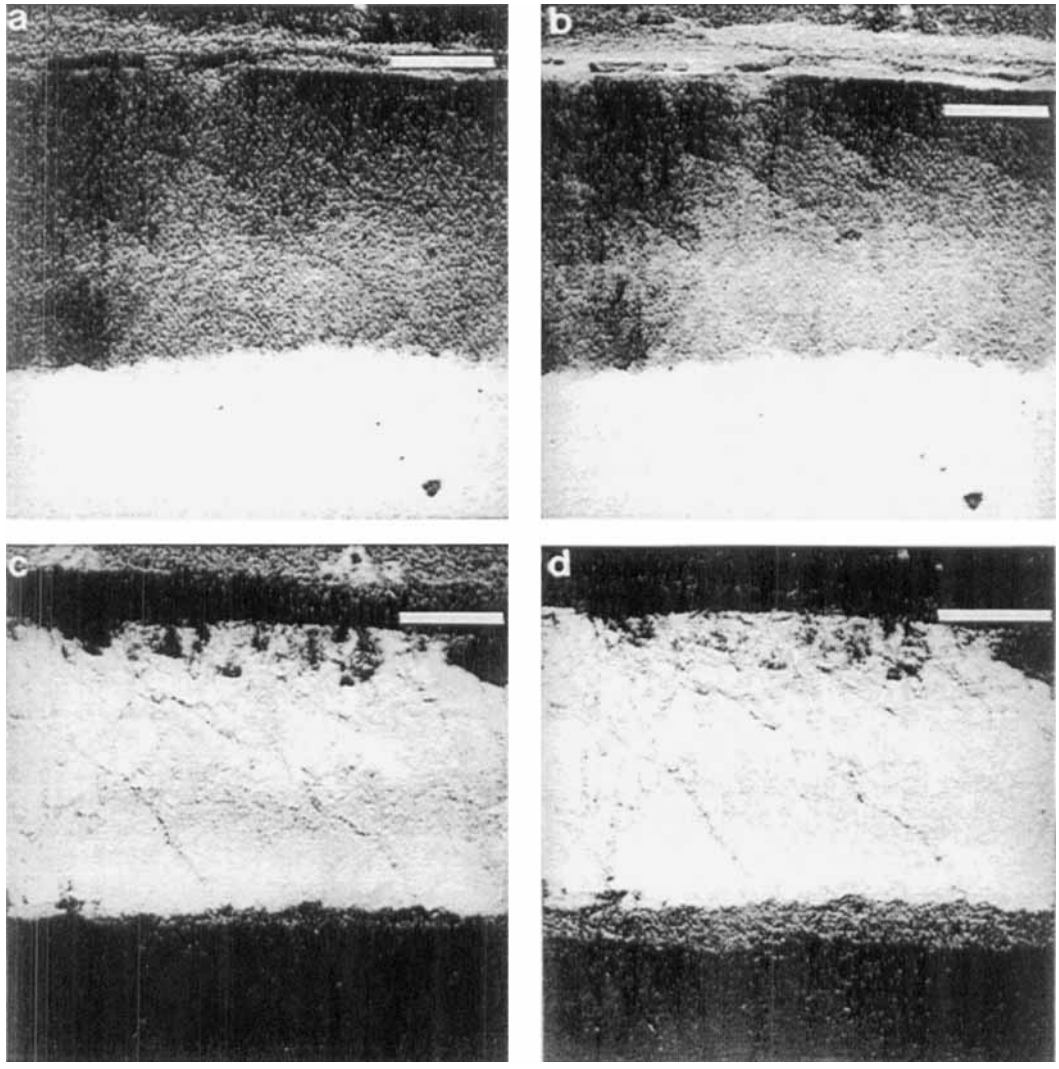

Fig. 4. Ion images of the bulk of enamel of a primary amelogenesis imperfecta tooth. 4a. A Ca^{2+} image showing a porous outer surface and a low ion yield from the inner part of the enamel corresponding to hypomineralized areas. 4b. An Na^{+} image with features similar to those of image a. 4c. A $(CN)^{-}$ image showing an inner enamel zone of high ion yield corresponding to organic remnants. 4d. A Cl^{-} image with an ion distribution similar to that of CN. The bars correspond to 150 µm.

SIMS imaging

In the SIMS images no patterns corresponding to the clinical classifications could be discerned. In the enamel of the tooth from family 48 the ion images of Ca^{2+} and Na^{+} demonstrated a porous outer surface with locally very low signals (Fig. 4a–d). In both images a lower ion yield was noted in the inner half of the enamel, more pronounced in the Na^{+} image. These areas correspond to the hypomineralized areas seen by polarized light microscopy. The $(CN)^{-}$ image of the sample, representing the organic component of enamel, showed an

Fig. 5. Secondary electron scanning ion microprobe image showing a disturbed enamel prism configuration in the deep hypomineralized enamel region. The bar corresponds to 150 μm.

inner zone of higher ion yield. Dark lines were seen extending from the dentinoenamel junction to the surface. The Cl^- image showed the same intensity distribution as the $(CN)^-$ image. The ISE SIM image (Fig. 5) showed changes in the prism configuration—that is, areas with less marked morphologic structure corresponding to the areas with a low ion yield for Ca^{2+} and Na^+.

In the tooth from family 44, images were obtained from the central part of the enamel with the wavy appearance (Fig. 6a–d). The Ca^{2+} image showed enamel prisms separated by areas with a low mineral content towards the surface. High Ca^{2+} signals were noted in the area adjacent to the dentinoenamel junction and in the boundaries of the central rough area visualized by an ISE SIM image (Fig. 7). In contrast to Ca^{2+}, signals from Na^+ were detected within the rough structure and not at its boundaries. In the rest of the examined area Na^+ was uniformly distributed. The $(CN)^-$ image demonstrated high ion yield in the borders of the rough structure and in the inner part of the enamel corresponding to the areas with high signals from Ca^{2+} and Na^+. The distribution of Cl^- was similar to that of $(CN)^-$. The ISE SIM image showed a whirling and irregular configuration of the prisms (Fig. 7).

SEM imaging

All teeth examined showed areas of hypomineralization in the enamel independent of clinical manifestation, clinical classification, or inheritance pattern. Further, the morphologic appearance was equivalent in those cases in which teeth were available from more than one family member. In the tooth from family 44, exhibiting enamel with a wavy appearance, the overviews showed a clear prism structure in the major part of the enamel with the exception of the outermost surface, which appeared structureless (Fig. 8a–c). In areas corresponding to the dark bands in the enamel the SEM images obtained by backscattered electrons showed a similar appearance with various dark and light bands. This contrast could possibly reflect variations in the elemental content of the enamel as the yield of backscattered electrons is sensitive to atomic number and hence to mineral content. In some areas the prisms at the enamel/dentin border appear oriented normally to this interface and extend to the enamel surface. However, especially in parts with a disturbed morphologic structure a keyhole pattern of the prisms was apparent.

For the tooth from family 29, with thick enamel, an area adjacent to the dentin/enamel border was examined, as was an area in the middle of the tooth (Fig. 9a–d). The overviews showed a normal enamel prism pattern close to the enamel/dentin border, which rapidly changed to an irregular prism pattern. At higher magnification sagitally and radially cut prisms were observed, with very marked prism borders.

Discussion

Most of the previously published papers concerning the histologic appearance of AI have been in the form of case reports, with only a few specimens from a limited number of patients. In no study has the clinical and histologic correlation been demonstrated.

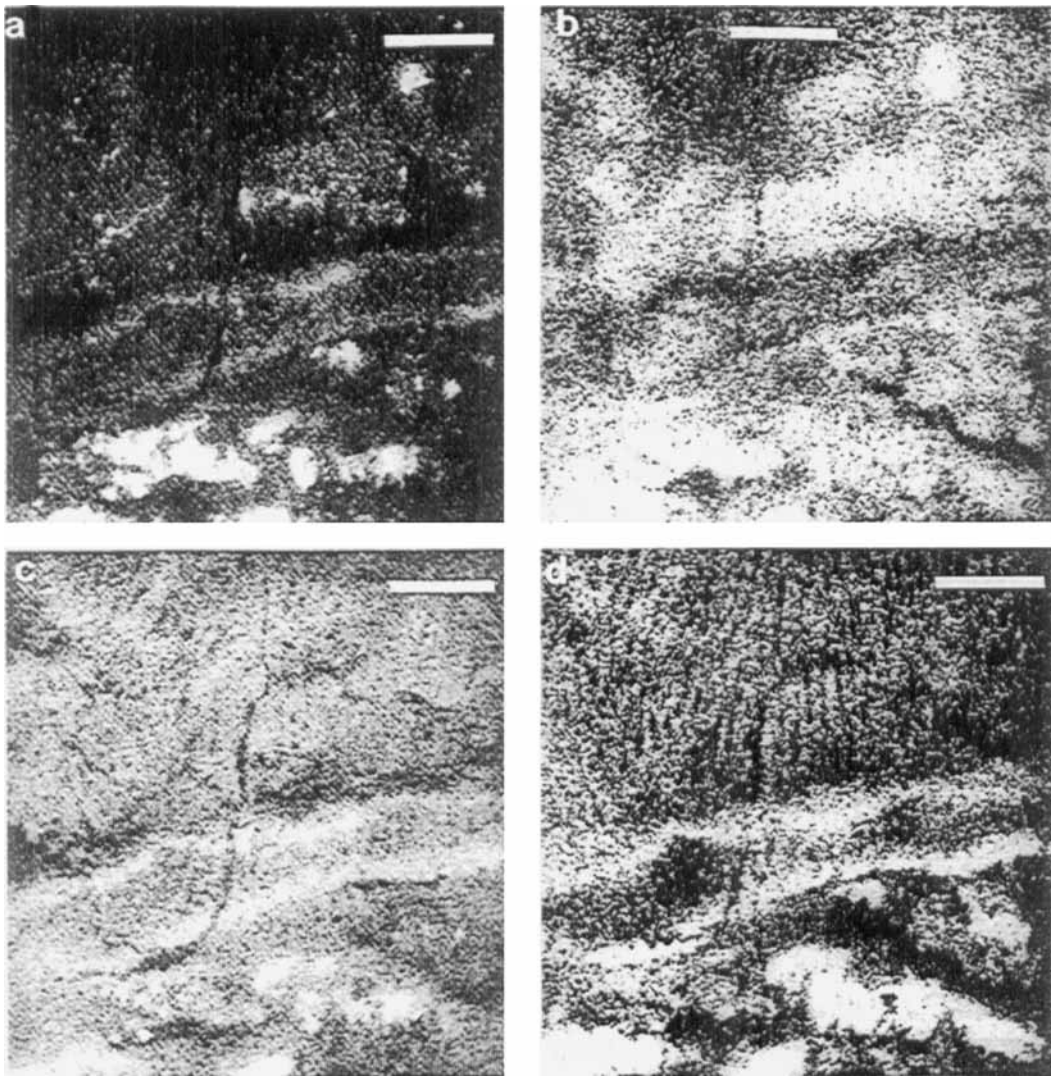

Fig. 6. Secondary ion mass spectrometry images of the same enamel bulk areas as in Fig. 5. 5a. A Ca^{2+} image showing a wavy appearance of enamel. Low mineral content regions are seen in parallel with the prisms. Close to dentin the signal intensity increased. 5b. The Na^{+} image shows an inverse ion yield pattern as compared with Ca^{2+}. 5c. In the $(CN)^{-}$ image a high signal intensity is demonstrated in the inner parts of the enamel corresponding to hypomineralization. 5d. The Cl^{-} distribution resembles that of CN. The bars correspond to 150 μm.

In the present study, with 16 patients, different histologic techniques have been applied, to give information on the histologic and chemotopographic characteristics of AI, in comparison to the clinical appearance of the disease.

The neonatal line seen in the ground sections of the AI teeth appeared positively birefringent, which is in accordance with earlier studies of normal primary teeth utilizing polarized light and microradiography, which showed the neonatal line as a hypomineralized band (33).

In the AI teeth an inner zone of hypomineralized enamel of various extents was found, with a thin but normally mineralized

Fig. 7. Secondary electron scanning ion microprobe image of amelogenesis imperfecta enamel showing a whirling and irregular configuration of prisms. The bar corresponds to 150 μm.

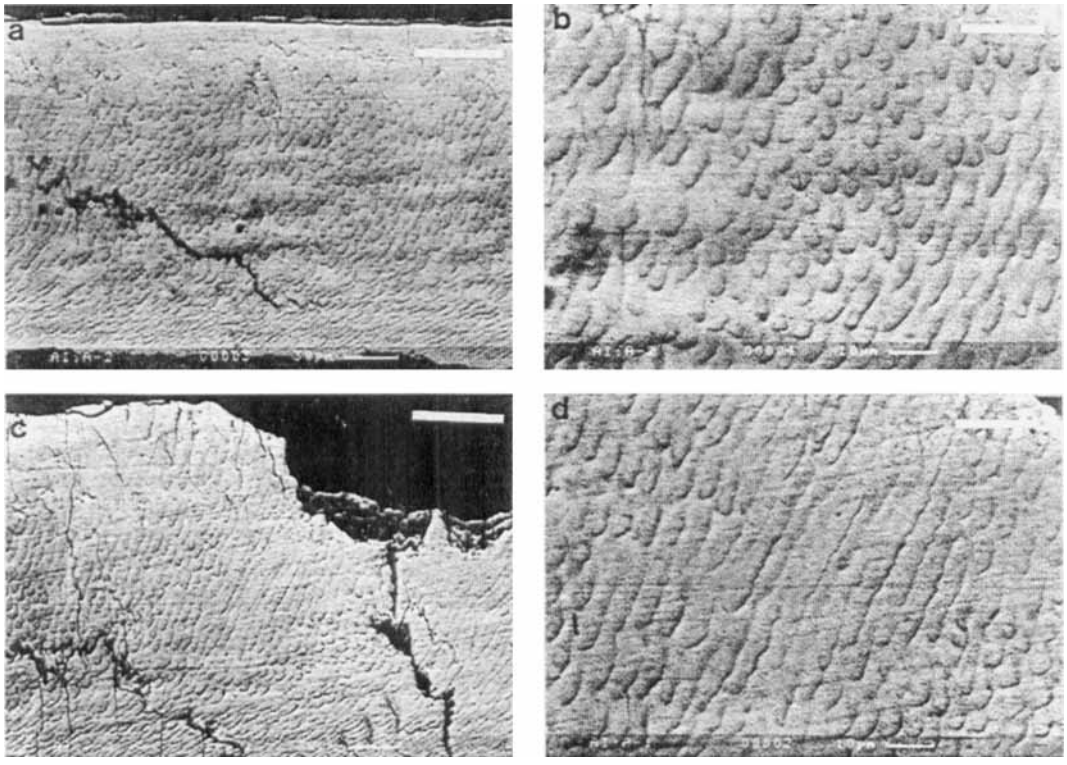

Fig. 8. Scanning electron microscopy images of amelogenesis imperfecta enamel exhibiting wavy enamel. 8a. Overview of a ground section, showing structureless enamel at the surface. 8b. A higher magnification of the central part of enamel, showing the prism configuration. 8c. Chipping off of the enamel surface layer. Fractures and irregularities are seen deep in the enamel. 8d. A higher magnification of the area just below the fractured surface. The bars correspond to either 50 or 20 μm.

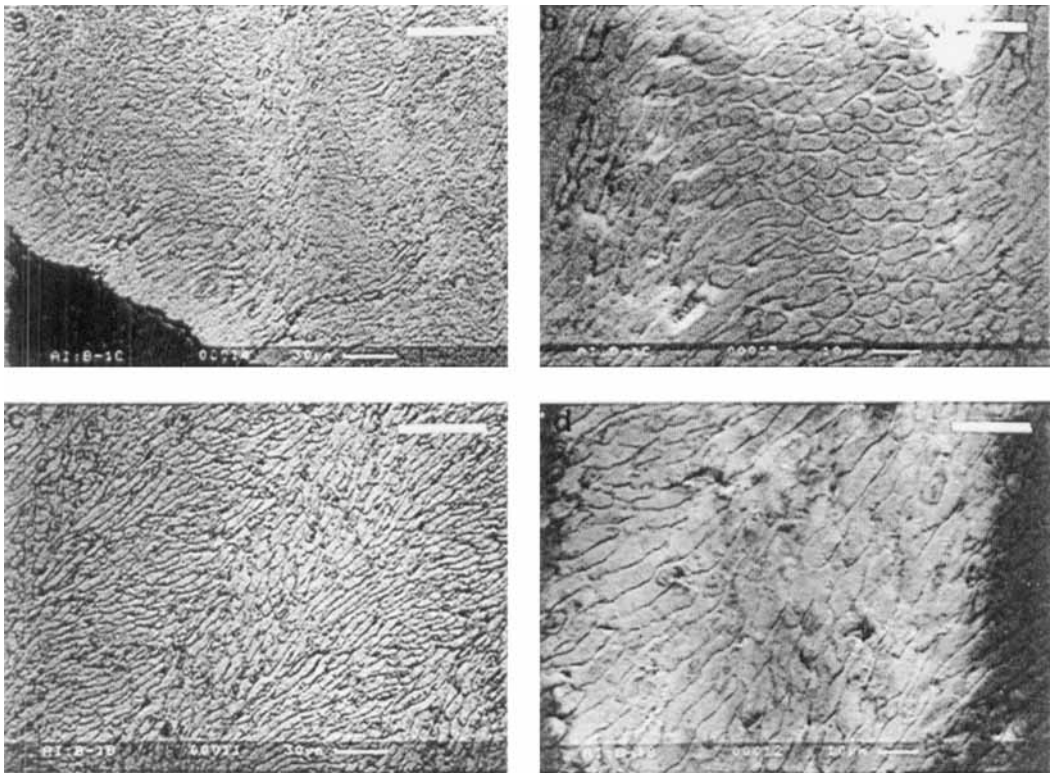

Fig. 9. SEM images from the section seen in Fig. 3, representing thick enamel. 9a. Image of the ground section from an area close to the enamel–dentin border; the dentin is seen at bottom left. The enamel prisms follow a very irregular pattern. 9b. In a higher magnification the irregular configuration of the prisms is clearly seen. 9c. Image of the bulk part of enamel showing the whirling prism pattern. 9d. The same area in a higher magnification. The bars correspond to either 50 or 20 μm.

surface zone. In ground sections of primary teeth from normal children, a hypomineralized or porous inner zone was also found (33); in the AI teeth, however, this zone was more extensive and pronounced. These findings are similar to the microradiographic observations by Bäckman & Anneroth in 1988 (15) but were, however, more distinct in their appearance on polarized light microscopy.

The enamel hypoplasia found in one case is not likely to be associated with AI per se but is, rather, related to an event around the time of birth. The defect showed no differences in the morphologic appearance compared with enamel hypoplasias from subjects without AI (33). According to the findings by Bäckman & Holm in 1986 (12), this subject had a medical record during the neonatal period which could well explain the occurrence of the enamel hypoplasia. Using polarization microscopy, no correlation could be found to the clinical classifications.

Chemotopographic studies or studies of the elemental composition of dental hard tissues have become useful tools in the understanding of the inorganic composition of enamel (34). The distribution pattern of the inorganic and organic elements and their relation to each other within normal and disturbed enamel is of relevance when trying to gain a deeper understanding of the processes behind the disturbed mineralization.

The hypomineralized areas in the bulk of the enamel correspond to regions in the SIMS images with high $(CN)^-$ signals, indi-

cating less inorganic material and thus relatively more organic material. As the content of inorganic material is lower than in normal enamel, it is tempting to believe that the organic content is higher than normal. This is supported by studies of decalcified sections of primary teeth (27) and by a previous paper in which the ion optic images of normal enamel showed a lower signal and also a more uniform appearance for CN^- (34). The enamel is evidently porous in this case and with a low content of inorganic matter. The porous outer surface has little resemblance to a normal enamel surface, and this finding is supported by earlier studies (15). The high resemblance between the $(CN)^-$ and the Cl^- images might possibly be explained by the fact that Cl^- partly reflects NaCl in the aqueous phase of the interprismatic reticulum.

The images of the section with hypomineralized and wavy enamel display a more irregular pattern for all elements analyzed in the AI specimens than normal enamel (34). The wavy bands appeared to be surrounded by higher ion yields of Ca^{2+}, whereas the bands themsleves exposed higher signals of Na^+. As the $(CN)^-$ and Cl^- signals were higher in the wavy areas, the hypomineralized appearance as seen in polarized light reflects a low degree of mineral content.

The polarized light and ion optic images suggest that the hypomineralized character of the primary enamel of the teeth investigated is related to a deficiency in the maturation stage of the enamel formation. Support for this suggestion is given by findings of Wright & Butler (35); they found that the enamel protein content in AI enamel was 5% compared with 0.1% in normal enamel. They proposed that the primary defect involves an abnormality in the mechanism for protein removal. This would thus explain the high ion yields for $(CN)^-$. As in the case with polarization microscopy, no correlation could be found to the clinical classifications when using SIMS.

The SEM images of the ground sections showed an irregular and whirling configuration in which the prisms were cut both sagittally and radially. The impression of an increased organic matter content from the polarized light microscopy and the SIMS images was strengthened by the SEM images. It is apparent that there is not only a changed mineral fraction, and thus possibly also changes in the mineral composition, but also structural changes of the morphology of the prisms, which is in agreement with the findings reported by Wright & Butler (35).

In the present study, irrespective of the clinical appearance or the inheritance pattern, the main findings were hypomineralized enamel with or without wavy bands. Neither of the analytical methods used in this paper distinguishes between the clinical phenotypes of AI. As can be seen from the histologic findings, it can be implied that the different clinical appearance rather reflects a difference in the expressivity of the disturbance. However, the subclassification might be useful as a clinical description.

Further studies of the ultrastructural level and of the chemical composition may increase the understanding of which factors influence the aberrations in the mineralization pattern of AI.

Acknowledgements.—This study was supported by a grant from the Lars Hiertas Minnesfond. At the University of Chicago, this research was supported by the National Science Foundation under grants DIR-8610518 and DIR-9017112.

References

1. Pindborg JJ. Aetiology of developmental enamel defects not related to fluorosis. Int Dent J 1982;32: 123–4.
2. Witkop CJ. Amelogenesis imperfecta, dentinogenesis imperfecta and dentin dysplasia revisited: problems in classification. J Oral Pathol 1989;17: 547–53.
3. Witkop CJ, Sauk JJ. Heritable defects of enamel. In: Stewart RE, Prescott GH, editors. Oro-facial genetics. St. Louis: Mosby, 1976.
4. Chosack A, Eidelman E, Wisotski J, Cohen T. Amelogenesis imperfecta among Israeli Jews and the description of a new type of local hypoplastic autosomal recessive amelogenesis imperfecta. Oral Surg 1979;1:148–56.
5. Bäckman B, Holmgren G. Amelogenesis imperfecta: a genetic study. Hum Hered 1988;38:189–206.
6. Bäckman B. Amelogenesis imperfecta—clinical manifestations in 51 families in a northern Swedish county. Scand J Dent Res 1988;96:505–16.

7. Lau EC, Slavkin HC, Snead ML. Analysis of human enamel genesis: insights into genetic disorders of enamel. Cleft Palate J 1990;27:121–130.
8. Lagerström M, Dahl N, Iselius L, Bäckman B, Petterson U. Mapping of the gene for X-linked amelogenesis imperfecta by linkage analysis. Am J Hum Genet 1990;46:120–5.
9. Lagerström M, Dahl N, Nakahori Y, et al. A deletion in the amelogenin gene causes X-linked amelogenesis imperfecta. Genomics 1991;10:971–5.
10. Witkop CJ. Hereditary defects in enamel and dentin. Acta Genet 1957;7:236–9.
11. Sundell S, Koch G. Hereditary amelogenesis imperfecta. Epidemiology and clinical classification in a Swedish child population. Swed Dent J 1985;9:157–71.
12. Bäckman B, Holm A-K. Amelogenesis imperfecta: prevalence and incidence in a northern Swedish county. Community Dent Oral Epidemiol 1986;14: 43–7.
13. Darling AI. Some observation on amelogenesis imperfecta and calcification of the dental enamel. Proc Roy Soc Med 1956;49:759–65.
14. Bergman G, Arwill T, Welander E, Wennström A. Observations on enamel and ectodermal lesions in some cases of amelogenesis imperfecta. Odontol Rev 1964;15:1–9.
15. Bäckman B, Anneroth G. Microradiographic study of amelogenesis imperfecta. Scand J Dent Res 1989;97: 316–29.
16. Schulze C. Erbbedingte Strukturanomalien menschlicher Zähne. Munich: Urban & Schwarzenberg, 1956.
17. Hals E. Hereditary enamel hypoplasia. Investigations of two families. Odontol Tidskr 1958;66: 562–82.
18. Hals E. Dentin and enamel anomalies: histologic observations. In: Witkop C, editor. Genetics and dental health. New York: McGraw-Hill Book Co, 1962.
19. Erpenstein von H, Wannemacher E. Schmelzhypoplasie und offener Biss als autosomal dominant vererbtes Merkmalspaar. Dtsch Zahnarztl Z 1968; 23:405–14.
20. Sauk JJ Jr, Vickers RA, Copeland JS, Lyon HW. The surface of genetically determined hypoplastic enamel in human teeth. Oral Surg 1972;34:60–8.
21. Sauk JJ Jr, Cotton WR, Lyon HW, Witkop CJ Jr. Electron-optic analyses of hypomineralized amelogenesis imperfecta in man. Arch Oral Biol 1972; 17:771–9.
22. Sauk JJ Jr, Lyon HW, Witkop CJ Jr. Electron optic microanalysis of two gene products in enamel heterozygous for X-linked hypomaturation amelogenesis imperfecta. Am J Hum Genet 1972;24: 267–76.
23. Kerebel B, Daculsi G. Ultrastructural study of amelogenesis imperfecta. Calcif Tiss Res 1977; 24:191–7.
24. Kerebel B, Dubois T. Etude critique de l'amelogenese imparfaite. Bull Group Int Rech Sci Stomatol Odontol 1982;25:291–311.
25. Wright JT. Analysis of a kindred with amelogenesis imperfecta. J Oral Pathol 1985;14:366–74.
26. Koray F, Soyman M, Erdogan G. Investigation of aetiopathogenesis of amelogenesis imperfecta through microscopic, submicroscopic and cytogenetic methods—a case report. J Oral Rehabil 1988;15:149–62.
27. Ooya K, Nalbandian J, Noikura T. Autosomal recessive rough hypoplastic amelogenesis imperfecta. Oral Surg 1988;65:449–58.
28. Bäckman B, Anneroth G, Hörstedt P. Amelogenesis imperfecta: a scanning electron microscopic and microradiographic study. J Oral Pathol Med 1989;18:140–5.
29. Levi-Setti R, Wang YL, Crow G. High spatial resolution SIMS with the UC-HRL scanning ion microprobe. J Physique 1984;45:C9-197-205.
30. Levi-Setti R, Crow G, Wang YL. Progress in high resolution scanning ion microscopy and secondary ion mass spectrometry imaging microanalysis. Scan Elect Microsc 1985;2:537–51.
31. Levi-Setti R, Wang YL, Crow G. Scanning ion microscopy: elemental maps at high lateral resolution. Appl Surf Sci 1986;26:249–64.
32. Norén JG, Engström C. Cutting of mineralized hard tissues with the Leitz low-speed saw microtome. Leitz Mitteilungen 1987;9:49–52.
33. Norén JG. Enamel structure in deciduous teeth from low-birth-weight infants. Acta Odontol Scand 1983;41:355–62.
34. Chabala JM, Edward S, Levi-Setti R, et al. Elemental imaging of dental hard tissues by secondary ion mass spectrometry. Swed Dent J 1988;12:210–2.
35. Wright JT, Butler WT. Alterations of enamel proteins in hypomaturation amelogenesis imperfecta. J Dent Res 1989;68:1328–30.

Received for publication 28 October 1992